Chalcogenide photonic crystal fiber for ultraflat mid-infrared supercontinuum generation

Sandeep Vyas[1,*], Takasumi Tanabe[2], Manish Tiwari[3], and Ghanshyam Singh[4]

[1]*Department of ECE, Vivekananda Institute of Technology (East), Jaipur 303012, India*
[2]*Department of EEE, Keio University, Kanagawa 2238521, Japan*
[3]*Department of ECE, Manipal University, Jaipur 303007, India*
[4]*Department of ECE, Malaviya National Institute of Technology, Jaipur 302017, India*
**Corresponding author: vyas.sandeep@vitej.ac.in*

Received June 1, 2016; accepted October 21, 2016; posted online November 22, 2016

In this Letter, we numerically simulate the generation of a 1–15 μm mid-infrared supercontinuum (SC) from a highly nonlinear $Ge_{11.5}As_{24}Se_{64.5}$-based photonic crystal fiber (PCF). This ultra-broadband SC is achieved in a 100 mm long PCF pumped using 85 fs laser pulses operated at 3.1 μm and a peak pulse power of 3 kW. The proposed design offers a flat dispersion profile with two zero dispersion wavelengths. This broad and flat dispersion profile of the $Ge_{11.5}As_{24}Se_{64.5}$ PCF, combined with the high nonlinearity (2474 $W^{-1}\,km^{-1}$), generates an ultra-broadband SC.

OCIS codes: 320.6629, 000.4430, 060.4370, 160.4330, 260.2030.
doi: 10.3788/COL201614.123201.

Fiber-based supercontinuum (SC) sources are the next generation light sources and one of the most attractive topic for researchers in the optics field. SC light has unique properties, namely, high brightness, wide spectral bandwidth, high coherence, and potential compactness[1]. SC sources in the mid-infrared (MIR) region find applications like sensing[2], optical coherence tomography (OCT)[3], frequency metrology[4], and molecular spectroscopy[5]. One of the remarkable applications of an SC is dense wavelength division multiplexing in telecommunication systems. An SC can be sliced into hundreds of channels of even transmission bandwidths of only a few terahertz[6]. SG generation (SCG) is normally lead off by pumping femto/picosecond pulses in the highly nonlinear photonic crystal fibers (PCFs) in the anomalous dispersion regime of the fiber and close to the zero-dispersion wavelength. Due to this, spectral broadening of the pulse occurs with the help of nonlinear effects such as self-phase modulation (SPM), modulation instability, and Raman scattering together with third- and higher-order dispersions. In the anomalous dispersion regime, the broadening mechanism is dominated by soliton dynamics. In this case, the breakup of the injected pulse is because of soliton fission, which is sensitive to input pulse fluctuations[1,7].

PCFs were originally proposed in the early seventies[8], although their significant development could be seen in the nineties when their fabrication became practically possible. The PCFs are classified in two categories. One is microstructured fibers (MOFs) whose light guidance is governed by a modified total internal reflection mechanism similar to that in conventional optical fibers, and another is photonic bandgap fibers (PBFs) in which light is confined within the core by the bandgap effect. MOFs also have applications in the field of laser and amplifier technology[9], are suitable for SCG due to low power requirements, and have allowed traditional fiber to go one step forward in generating supercontinua. Practically, the possibility of tailoring the dispersion profile combined with the tight confinement of the propagating mode enhance the nonlinear effects that are responsible for enhancement of the SC spectrum[7]. The dispersion slope and nonlinearity can be controlled by varying the air hole diameter (d) and the hole-to-hole spacing (Λ). With this controllability, we can achieve many important and practical applications in optical communication systems, dispersion compensation, and nonlinear optics that are difficult to be achieved with conventional optical fibers. With PCFs, we can also achieve ultra-flattened[10].

Initially, the SCG was demonstrated with silica material. In silica fibers, SC broadening is limited beyond the 2.5 μm wavelength due to the limited transparency window of silica[11]. However, to expand this bandwidth, researchers are required to extend the range of the SC from the near-infrared region (NIR) to the MIR (3–20 μm). SC has many applications in military, medical, biological, and sensing systems with the MIR[12]. Silica material has its limitations so new alternative materials are required with larger transmission windows and high nonlinearity. Some of the existing non-silica material for SCG are lead silicate, bismuth oxide, fluoride, tellurite, and chalcogenide glass[13–15]. In recent years chalcogenide glasses have been reported as promising nonlinear materials in the MIR. The chalcogenide glasses are most suitable in the MIR region because of their higher nonlinearity and wider transmission window, up to 25 μm, as compared to the above-mentioned materials[16]. In the above-mentioned materials, except chalcogenide, all materials have an uncontrollable propagation loss beyond the 5 μm wavelength[17].

Some of existing chalcogenide materials are mostly used by researchers for SCG in MIR, like As_2S_3, As_2Se_3,

$Ge_{11.5}As_{24}S_{64.5}$, and $Ge_{11.5}As_{24}Se_{64.5}$. In all chalcogenide materials, the $Ge_{11.5}As_{24}Se_{64.5}$ material governs by comparatively high third-order nonlinearity. $Ge_{11.5}As_{24}Se_{64.5}$ has drawn attention not only because of its high thermal and optical stability but also its excellent film-forming properties under intense illumination[18].

Recently, $Ge_{11.5}As_{24}Se_{64.5}$-based chalcogenide glasses have been investigated by several researchers. In 2010, Gai *et al.*[19] fabricated 600 nm × 500 nm nanowires from $Ge_{11.5}As_{24}Se_{64.5}$ material for SCG around 1.0 to 2.2 μm with 18 mm long nanowires and determined nonlinear coefficient $(\gamma) \approx 136 \pm 7\ \mathrm{W^{-1}\,m^{-1}}$ at 1.55 μm. In 2011, Spurny *et al.*[20] demonstrated fabrication techniques of PCF for $Ge_{11.5}As_{24}Se_{64.5}$-based chalcogenide glass. In 2014, Karim *et al.*[21] reported numerically simulated results with five different nanowire structures with width ranges of 0.7 to 0.8 μm and achieved SCs up to 4.6 μm. In 2015, Sakunasinha *et al.*[22] reported simulation results of the $Ge_{11.5}As_{24}Se_{64.5}$ material using MgF_2 for the lower cladding of the chalcogenide waveguide SCG, about 1.3 to 3.3 μm with a 1 cm length waveguide, and in 2015, Karim *et al.*[18] showed an optimized waveguide using MgF_2 glass for its lower cladding and the SC spectrum extending in the wavelength range of 1.8 to 11 μm. In 2015, Karim *et al.*[17] showed their results with MOFs and achieve SC spectrum from 1.3 μm to somewhere around 12 μm. Recently, we proposed a PCF with $Ge_{11.5}As_{24}Se_{64.5}$-based chalcogenide glass that enables us to extend the SC up to 10 μm[23].

In this Letter, we propose a PCF design that gives the following improvements. (1) A flatter dispersion below 100 ps/km/nm. (2) Two zero dispersion wavelengths (ZDWs) at 2.9 and 13.1 μm. (3) Ultra-flat SCG ranging from 1 to 15 μm.

This Letter is organized as follows. First, we concisely analyze the modal properties of the $Ge_{11.5}As_{24}Se_{64.5}$-based chalcogenide PCF. We have calculated the material dispersion using the second-order Sellmeier formula for the material and a full modal investigation of the optical parameters of the PCF is in terms of the refractive index, the chromatic dispersion (D_c), the effective area (A_{eff}), the nonlinear coefficient (γ), and confinement loss. Next, we present results on SCG in few millimeters (mm) of $Ge_{11.5}As_{24}Se_{64.5}$-based chalcogenide PCF. We have used the generalized nonlinear Schrödinger equation (GNLSE) to simulate SCG.

Here, we are using the finite-difference time-domain method to analyze the optical properties of PCF. Chromatic dispersion $D_c\,(\lambda)$ can be calculated using the relation

$$D_c(\lambda) = -\frac{\lambda}{c}\frac{d^2 n_{\mathrm{eff}}}{d\lambda^2}, \tag{1}$$

where λ is the operating wavelength, c is the speed of light in vacuum, n_{eff} is the real part of the effective index. Here, $n_{\mathrm{eff}} = \lambda\beta/2\pi$ and β is the propagation constant[7]. We can calculate the wavelength-dependent refractive index of $Ge_{11.5}As_{24}Se_{64.5}$-based chalcogenide glass by following the Sellmeier equation[23],

$$n^2(\lambda) = 1 + \frac{5.78525\lambda^2}{\lambda^2 - 0.28795^2} + \frac{0.39705\lambda^2}{\lambda^2 - 30.39338^2}. \tag{2}$$

We can evaluate the nonlinear coefficient (γ) given by[7]

$$\gamma = \frac{2\pi n_2}{\lambda A_{\mathrm{eff}}}, \tag{3}$$

where the nonlinear refractive index of the material is n_2, the pump wavelength is λ, and effective area of the fundamental mode is A_{eff}. Here, the $Ge_{11.5}As_{24}Se_{64.5}$-based chalcogenide glass has $n_2 = 4.3 \times 10^{-18}\ \mathrm{m^2/W}$ at 3.1 μm[23]. In the PCF the effective area of the propagating mode (A_{eff}) can be calculated by[7]

$$A_{\mathrm{eff}} = \frac{\left(\iint_{-\infty}^{\infty} |E|^2 \mathrm{d}x\mathrm{d}y\right)^2}{\iint_{-\infty}^{\infty} |E|^4 \mathrm{d}x\mathrm{d}y}, \tag{4}$$

where the electric field distribution is E. The confinement loss is calculated by the relation[7] $\mathrm{CL} = 8.686\ k_0\,\mathrm{Im}(n_{\mathrm{eff}})$, where the imaginary part of the effective refractive index is $\mathrm{Im}(n_{\mathrm{eff}})$ and $k_0 = 2\pi/\lambda$ is the wavenumber in free space[24].

The pulse propagation in the PCF is numerically described by the following GNLSE. This equation has been solved for the output pulse envelope $[A(z,t)]$ using the split-step Fourier method,

$$\frac{\partial A}{\partial z} + \frac{\alpha}{2}A - \left(\sum_{n\geq 2}\beta_n \frac{i^{n+1}}{n!}\frac{\partial^n A}{\partial t^n}\right) = i\gamma\left(1 + \frac{i}{\omega_o}\frac{\partial}{\partial t}\right)\left[A(z,t)\int_{-\infty}^{\infty} R(t')|A(z,t-t')|^2 \mathrm{d}t'\right], \tag{5}$$

where the envelope of the optical field is $A(z,t)$, time is t, the nth derivative of the propagation constant β is β_n, the nonlinear coefficient is γ, the distance is z, and the retarded time travelling at the envelope group velocity is τ[7].

The Raman response function of the material, including the instantaneous electronic and vibrational Raman contributions, is described by[7]

$$R(t) = (1 - f_r)\delta(t) + f_r h_R(t). \tag{6}$$

We know that the optical properties of chalcogenide materials are governed by photoinduced effects, namely, photodarkening and photoinduced anisotropy. Therefore, the response time and the third-order susceptibility $(\chi^{(3)})$ will change[25]. The temporal Raman response $[h_R(t)]$ dependence on the Raman gain spectrum can be expressed as[26]

$$g_R(f) = \frac{2\omega_p}{c} n_2 f_r\,\mathrm{Im}[H_R(f)], \tag{7}$$

where the pump frequency is ω_p, $\mathrm{Im}[H_R(f)]$ is the imaginary part of the Fourier transform of $h_R(t)$[18], and $h_R(t)$ is calculated as

$$h_R(t) = \frac{\tau_1^2 + \tau_2^2}{\tau_1 \tau_2^2} \exp\left(-\frac{t}{\tau_2}\right) \sin\left(\frac{t}{\tau_1}\right). \tag{8}$$

where $\tau_1 = 15.5$ fs and $\tau_2 = 230.5$ fs for $Ge_{11.5}As_{24}Se_{64.5}$-based glasses. They are chosen to provide a good fit with the Lorentzian spectral profile. We can calculate fraction f_r by the Kramers–Kroning relation[26]. It comes out to be equal to 0.031[18]. The Kramers–Kroning relation can be expressed as

$$f_r = \frac{\lambda}{2\pi^2 n_2} \int_0^\infty \frac{g_R(f)}{f} \mathrm{d}f. \tag{9}$$

In this Letter, we are considering the hyperbolic secant pulse as the input pulse and can be expressed as

$$A(z = 0, t) = \sqrt{P_0}\, \mathrm{sech}\left(\frac{t}{t_0}\right) \exp\left(-i \frac{C}{2} \frac{t^2}{t_0^2}\right), \tag{10}$$

where $t_0 = t_{\mathrm{FWHM}}/1.7627$ and the peak power of input pulse is P_0.

Here, laser polarization also plays an important role in SCG. The circularly polarized laser pulses generate a smaller SC in comparison with linearly polarized pulses[27].

The $Ge_{11.5}As_{24}Se_{64.5}$-based chalcogenide PCF fiber is the best choice for SCG because of its high nonlinearity coefficient (γ). We have designed a $Ge_{11.5}As_{24}Se_{64.5}$-based PCF that is suitable for SCG at 3.1 μm pumping. In this Letter, we have improved our previous design to achieve a flatter dispersion profile[23]. In our proposed design, the dispersion tailoring has been done very carefully to achieve the desirable dispersion characteristics. The cross section of the basic layout has been displayed in Fig. 1. The electric field distribution of the propagating mode is shown in Fig. 2, which proposes that the fiber is a single mode fiber.

Here, the PCF is a 5-ring structure; when we move outward to the center first ring of air holes is denoted by d_1 and pitch is denoted by Λ_1; sequentially, the last ring of air holes is denoted by d_5 and the pitch is denoted by Λ_5. The values of Λ_1 to Λ_5 and d_1/Λ_1 to d_5/Λ_5 are shown in Table 1.

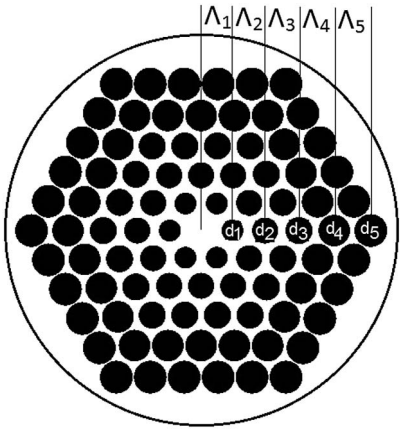

Fig. 1. Structure of the hexagonal PCF.

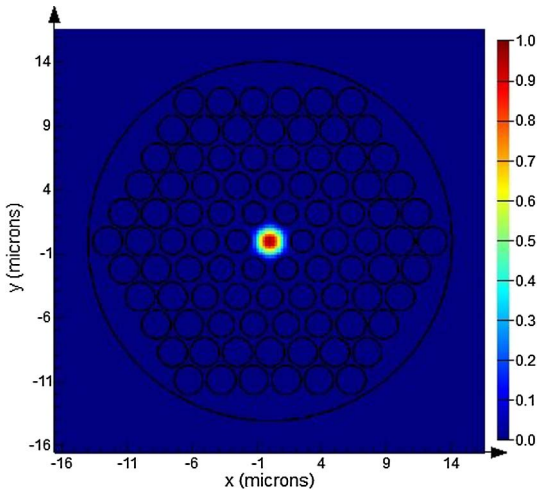

Fig. 2. Electric field distribution of the propagating mode at 3.1 μm.

The variation in the chromatic dispersion with the wavelength of the proposed fiber has been demonstrated in Fig. 2. By carefully choosing the pitch (Λ) and the air hole diameter (d), we find a flat dispersion profile from about 2 to 15 μm with two ZDWs, 2.9 and 13.1 μm. Here, the starting pitch size is small and the pitch length is regularly increased when we move upward. The smaller pitch sizes nearer to the center help to minimize the effective area (A_{eff}) and the longer pitch values in the outward direction help to maintain a flat dispersion profile from the longer wavelength side. SCG can be maximized by achieving a low and flat dispersion profile. It can reduce the temporal walk-off effect at the time of the spectral broadening process[28]. The pump wavelength of 3.1 μm is in the anomalous dispersion region. In Fig. 3 the, black solid line shows the material dispersion, the dashed line shows the chromatic dispersion, and the dashed-dot line shows the β_2 of the proposed PCF.

The wavelength-dependent effective area (A_{eff}) of the propagating mode and the compatible nonlinear coefficient (γ) are illustrated in Fig. 4. Numerically calculated values of effective area (A_{eff}) and nonlinear coefficient (γ) are 3.5241 μm^2 and 2474 $W^{-1}\,km^{-1}$.

In Fig. 5, the confinement loss of the PCF is shown with respect to the wavelength. $Ge_{11.5}As_{24}Se_{64.5}$ is the low-loss material[29], the confinement loss is 3.65×10^{-10} dB/m, and the propagation loss is 0.68 dB/m at a pump wavelength of 3.1 μm. For the proposed PCF, the confinement loss is meaningful at long wavelengths above ~11 μm.

The GNLSE is solved by the split-step Fourier method[7]. We have taken 100 mm long PCF. In the numerical simulation, we pumped sech optical pulses at 3.1 μm wavelength. The typical value of the effective area (A_{eff}) is 3.5241 μm^2 and the nonlinear coefficient (γ) is 2474 $W^{-1}\,km^{-1}$ at a pump wavelength of 3.1 μm, which is in the anomalous dispersion regime. The PCF has a very flat dispersion from 2 to 15 μm (Fig. 3). The anomalous regime pumping increases the spectral broadening in

Table 1. Designing Parameters of PCFs

Chalcogenide crystals ($Ge_{11.5}As_{24}Se_{64.5}$)	Rings	Λ_1	Λ_2	Λ_3	Λ_4	Λ_5	d_1/Λ_1	d_2/Λ_2	d_3/Λ_3	d_4/Λ_4	d_5/Λ_5
PCF	5	2.4 μm	2.5 μm	2.6 μm	2.7 μm	2.8 μm	0.7	0.8	0.8	0.9	0.9

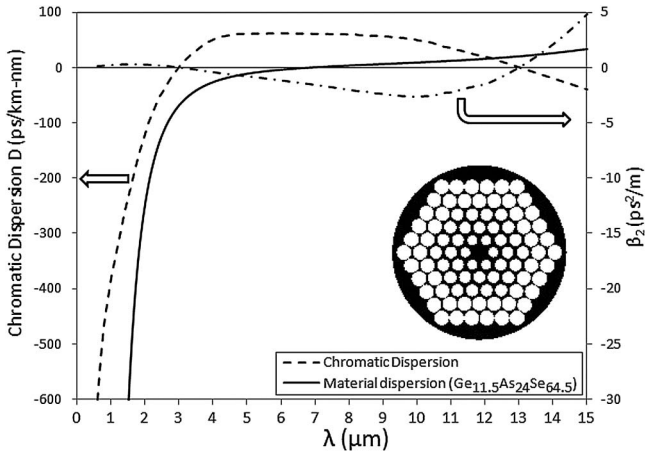

Fig. 3. Dispersion curves of the proposed $Ge_{11.5}As_{24}Se_{64.5}$ glass PCFs.

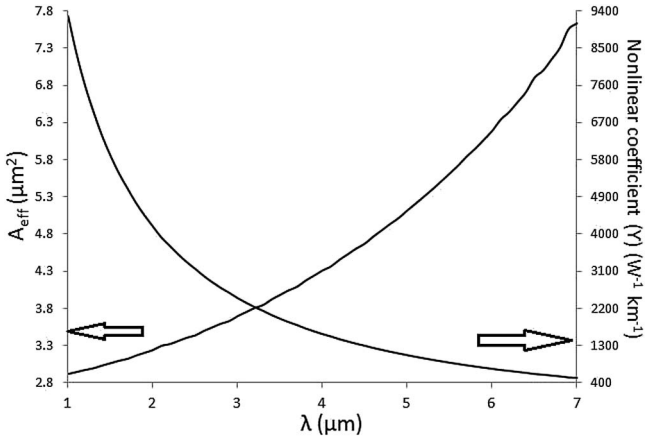

Fig. 4. Effective area and corresponding nonlinear coefficient.

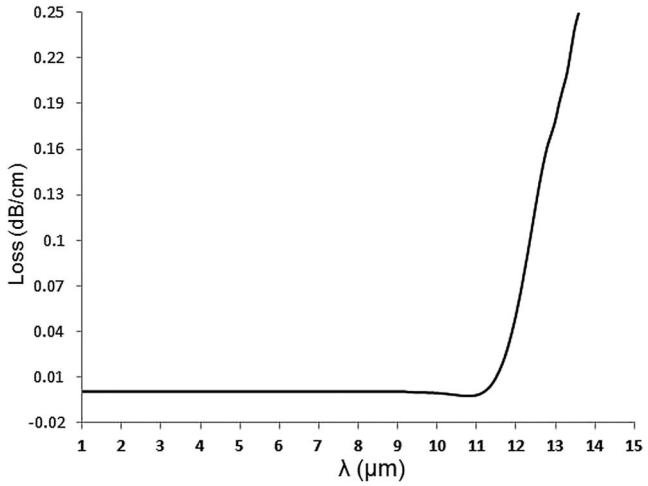

Fig. 5. Confinement loss of the propagating mode of the proposed fiber.

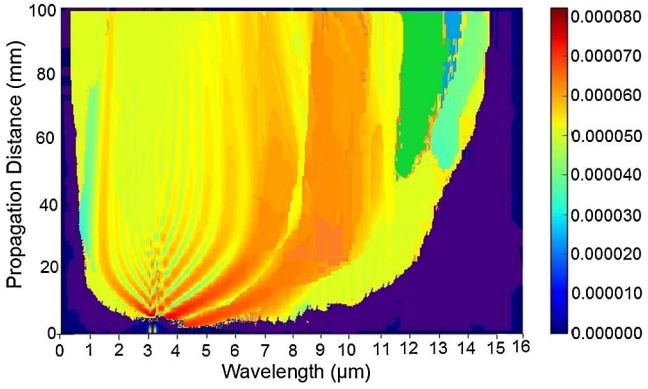

Fig. 6. Spectral escalation of the SC in PCF (spectral intensity in dB, scale bar on the right).

the long wavelength side, which is mainly caused by soliton fission and Raman soliton self-frequency shift. The initial broadening happens because of four-wave mixing. After that, further propagation increases the spectral broadening in the long wavelength side, mainly caused by Raman solution self-frequency shift and soliton fission, along the generation of the analogous dispersive waves on the short-wavelength side of the ZDW, which ultimately merge into a broad SC spectrum[28]. The extraordinary broadening is possible in the anomalous dispersion regime only by soliton dynamics. In soliton fission, the input pulse splits up into a series of consequent soliton pulses, each pulse exhibiting its unique temporal and spectral properties that are very susceptible to pump pulse shot noise[30].

The pulse duration is 85 fs (FWHM) with a 160 kHz repetition rate[31,32], and the input peak power is 3 kW. The spectral spans of SCG in the PCF with peak powers of 3 kW are shown in Fig. 6. The spectral escalation of the 3 kW input pulse for different lengths is shown in Fig. 7. Figure 6 shows that SC spectral broadening is from 1 to 15 μm. The spectral power density is 74.67 mW/nm (average) at the end of the fiber.

In conclusion, we numerically simulate SCG in a 100 mm long $Ge_{11.5}As_{24}Se_{64.5}$ glass-based solid core PCF with hexagonal cladding of air holes. We design a PCF to achieve a flat dispersion from 2 to 15 μm. The typical values of the accomplishable nonlinear coefficient (γ), effective area (A_{eff}), and dispersion at the wavelength

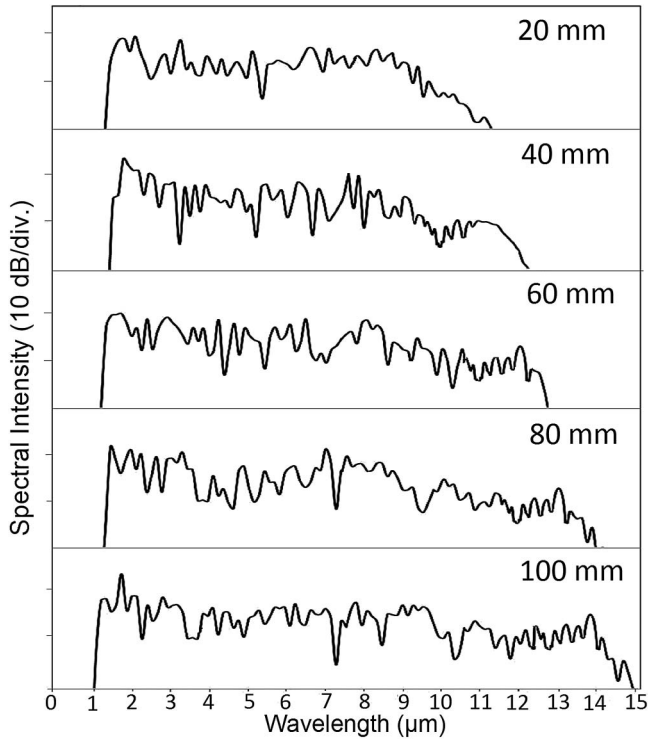

Fig. 7. Spectra of the SC for different lengths.

(λ) 3.1 μm are 2474 $W^{-1}\,km^{-1}$, 3.5241 μm^2, and 8.014 ps/km/nm, respectively. The PCF is employed for numerical simulation of SCG using 85 fs pump pulses of 3 kW peak power at a wavelength of 3.1 μm. IConsequently, the SC bandwidth is 1 to 15 μm for a 3 kW peak power.

The authors gratefully acknowledge the grants available by the India–Japan Cooperative Science Programme awarded jointly to MNIT Jaipur and KEIO University, Hiyoshi Campus, Japan (Project sanction number: DST/INT/JSPS/P-180/2014).

References

1. J. M. Dudley, G. Genty, and S. Coen, Rev. Mod. Phys. **78**, 1135 (2006).
2. T. M. Monro, W. Belardi, K. Furusawa, J. C. Baggett, N. G. R. Broderick, and D. J. Richardson, Meas. Sci. Technol. **12**, 854 (2001).
3. D. L. Marks, A. L. Oldenburg, J. J. Reynolds, and S. A. Boppart, Opt. Lett. **27**, 2010 (2002).
4. S. T. Cundiff and J. Ye, Rev. Mod. Phys. **75**, 325 (2003).
5. M. J. Thorpe, D. D. Hudson, K. D. Moll, J. Lasri, and J. Ye, Opt. Lett. **32**, 307 (2007).
6. O. Boyraz, J. Kim, M. N. Islam, F. Coppinger, and B. Jalali, J. Lightwave Technol. **18**, 2167 (2000).
7. G. P. Agarwal, *Nonlinear Fiber Optics*, 4th ed. (Academic, 2007).
8. P. Kaiser, E. A. J. Marcatili, and S. E. Miller, Bell Syst. Tech. J. **52**, 265 (1973).
9. J. Wallace, Laser Focus World **37**, 20 (2001).
10. W. H. Reeves, J. C. Knight, P. St. J. Russell, and P. J. Roberts, Opt. Express **10**, 609 (2002).
11. T. Cheng, K. Nanasaka, T. H. Tuan, X. Xue, M. Matsumoto, H. Tezuka, T. Suzuki, and Y. Ohishi, Opt. Lett. **41**, 2117 (2016).
12. J. S. Sanghera, L. B. Shaw, and I. D. Aggarwal, IEEE J. Sel. Top. Quantum Electron. **15**, 114 (2009).
13. A. Agrawal, M. Tiwari, Y. O. Azabi, V. Janyani, B. M. A. Rahman, and K. T. V. Grattan, J. Mod. Opt. **60**, 956 (2013).
14. W. Yuan, Laser Phys. Lett. **12**, 125101 (2015).
15. C. R. Petersen, U. Møller, I. Kubat, B. Zhou, S. Dupont, J. Ramsay, T. Benson, S. Sujecki, N. Abdel-Moneim, Z. Tang, D. Furniss, A. Seddon, and O. Bang, Nat. Photonics **8**, 830 (2014).
16. V. Shiryaev and M. Churbanov, J. Non-Cryst. Solids **377**, 225 (2013).
17. M. R. Karim, B. M. A. Rahman, Y. O. Azabi, A. Agrawal, and G. P. Agrawal, J. Opt. Soc. Am. B **32**, 2343 (2015).
18. M. R. Karim, B. M. A. Rahman, and G. P. Agrawal, Opt. Express **23**, 6903 (2015).
19. X. Gai, S. Madden, D. Choi, D. Bulla, and B. L. Davies, Opt. Express **18**, 18866 (2010).
20. M. Spurny, "Photonic crystal waveguides in chalcogenide glasses fiber," https://core.ac.uk/download/files/95/1586610.pdf (2011).
21. M. R. Karim, B. M. A. Rahman, and G. P. Agrawal, Opt. Express **22**, 31029 (2014).
22. P. Sakunasinha, S. Suwanarat, and S. Chiangga, Proc. SPIE **9659**, 96591J (2015).
23. S. Vyas, T. Tanabe, G. Singh, and M. Tiwari, in *IEEE International Conference on Computational Techniques in Information and Communication Technologies (ICCTICT)* (2016), p. 607.
24. F. Poli, *Photonic Crystal Fibers Properties and Applications* (Springer, 2007).
25. A. B. Salem, R. Cherif, and M. Zghal, in *Progress in Electromagnetics Research Symposium Proceedings*, Marrakesh, Morocco, March 20–23 (2011).
26. F. X. Kärtner, D. J. Dougherty, H. A. Haus, and E. P. Ippen, J. Opt. Soc. Am. B **11**, 1267 (1994).
27. S. Rostami, M. Chini, K. Lim, J. P. Palastro, M. Durand, J. C. Diels, L. Arissian, M. Baudelet, and M. Richardson, Sci. Rep. **6**, 1 (2016).
28. W. Yuan, Laser Phys. Lett. **10**, 095107 (2013).
29. B. Zhang, W. Guo, Y. Yu, C. Zhai, S. Qi, A. Yang, L. Li, Z. Yang, R. Wang, D. Tang, G. Tao, and B. L. Davies, J. Am. Ceram. Soc. **98**, 1389 (2015).
30. A. Hartung, A. M. Heidt, and H. Bartelt, Opt. Express **19**, 7742 (2011).
31. A. Thai, M. Hemmer, P. K. Bates, O. Chalus, and J. Biegert, Opt. Lett. **36**, 3918 (2011).
32. F. Silva, D. R. Austin, A. Thai, M. Baudisch, M. Hemmer, D. Faccio, A. Couairon, and J. Biegert, Nat. Commun. **3**, 807 (2012).